Evidence of chromium-cobalt binary cluster formation by pulsed laser evaporation

Andrei Burnin[1], Joseph J. BelBruno[1], Ursula J. Gibson[1,2]*

[1]Dept. of Chemistry, Dartmouth College, Hanover NH 03755, USA Dept. of Physics, Norwegian

[2]University of Science and Technology, N7491 Trondheim, Norway

Keywords: binary clusters, transition metals, mass spectrometry

Abstract

Intermetallic clusters are observed in the Co-Cr system. We report on the use of time of flight mass spectroscopy to investigate the cluster spectrum resulting from Nd-YAG ablation of a Co-Cr target. Cr^+ clusters dominated the spectrum, with Co^+ clusters as the second most intense peak, and we found a clearly resolved Cr-Co binary cluster that could be suitable for co-doping during the growth of laser crystals. Significant contributions from elemental dimers as well as some oxide clusters were also observed. Density functional calculations indicated that formation of the observed intermetallic clusters was thermodynamically favorable.

1. INTRODUCTION

Development of lasers in the mid-infrared region is a topic of great interest, due to applications in medical and environmental diagnostics[1]. Many biomolecules have distinct signatures in this region, and the absence of water absorption between 3 and 5 μm makes this region particularly interesting for

diagnostic applications[2]. One of the promising candidates for broadband operation in this region is Cr:ZnS[3]. As with rare-earth fiber lasers, high concentrations of dopants are desired[4], but clustering effects are deleterious[5]. In rare-earth systems, co-doping, e.g. Al with Tm, has been shown to reduce clustering due to the formation of bridging Al-O-Tm complexes[6,7]. Recently, Yan et al.[8] reported that co-doping of Cr and Co in ZnO may reduce Cr clustering. Additionally, control over the clustering of magnetic elements may be important in room temperature dilute magnetic semiconductors[8]. In this paper, we explore laser ablation generation of intermetallic clusters as a possible method for introducing dopants pairwise into a host semiconductor. Laser ablation has been used for the deposition of many materials, and is routinely used as a method of generating clusters both for film deposition and for mass spectroscopic studies.

Mass spectroscopy following laser ablation is used to verify first principles cluster formation calculations and has resulted in the discovery of "magic clusters" with high stability, such as lithium[9] 2, 8 and 20 and carbon clusters[10]. Theoretical and experimental cluster studies have also been made on more complex materials, including II-VI semiconductors[11], silicides[12,13] and some copper[14] and aluminum compounds[15,16], among others. Intermediate between the mixed covalent-ionic bonding of II-VI materials, and the purely metallic bonding of noble metal clusters lies an interesting regime where the formation of intermetallic compounds is observed in the bulk phase diagram. Few reports of clusters in these systems can be found in the literature[17–19], and transition metal binary clusters appear not to have been studied. However, transition metal pairs are of emerging interest for their charge transfer properties for infrared laser sources[20,21].

We chose Co and Cr for this study because of the potential for doping applications[8] and the existence of the broad phase field of the σ (1:1) intermetallic compound in the bulk phase diagram suggests that it should be possible to form stable two-atom mixed clusters. Density functional calculations support this conclusion. We used laser ablation for the production of

cobalt-chromium clusters, which would permit incorporation of such a source, combined with a quadrupole mass analyzer, in a deposition system for directly co-locating the desired dopants during growth of a thin-film material.

2. MATERIALS AND METHODS

2.1. Sample preparation. The targets for laser ablation were prepared from a binary alloy containing 50/50 *at. %* of chromium and cobalt as following. First, 10.4 *g* of 99.99% pure chromium pieces (Alpha Aesar) and 11.8 *g* of 99.5% pure cobalt shots (Alpha Aesar) were mixed in a cleaned new copper die, which was then placed into an arc-melter chamber. The copper die provided efficient thermal contact with the water-cooled base of the apparatus. In order to displace the residual air in the chamber, it was evacuated using a mechanical vacuum pump and filled to 1 *atm* of argon sequentially three times. The melting process in the apparatus was monitored through a neutral density optical filter. After the arc-discharge was initiated it was sustained for about 3 *min*. The initially formed alloy ingot was cooled, flipped and melted again for another 3 *min* period in order to ensure homogeneity in composition. Then, the arc-melter was left to cool down for 30 *min* before opening the chamber and removing the ingot. The resultant alloy specimen was about 2.5 *cm* in diameter and 5 *mm* thick. Finally, the ablation targets were cut out of the ingot using a diamond saw. Freshly cut surfaces were too reflective for laser ablation. In order to alleviate this, the surface was roughened using 220 grit sandpaper.

2.2. Mass-spectrometry. The prepared 50/50 *at.%* chromium/cobalt alloy ablation target was loaded into the ablation chamber of the dual-acceleration stage time-of-flight (TOF) mass-spectrometer (MS) described previously[22]. Upon reaching a base pressure of $3.5 \cdot 10^{-6}$ *Torr*, the

sample was targeted with a Q-switched Nd:YAG pulsed laser (Spectra Physics DCR-11) operated at a 10 *Hz* repetition rate. The laser dual wavelength (1064 and 532 *nm*) beam was focused on the target through a 50 cm focal length quartz lens. This provided combined fluences up to 4.5 $J \cdot cm^{-2}$ in a 10 ns pulse to produce a plasma plume of ions and neutrals. Post formation, the clusters equilibrated and spatially spread through the extraction region between two sets of grids. A short electric pulse delayed by 30 ms from the laser pulse was applied to the grids to extract the ions orthogonally into the acceleration region. The second electric pulse accelerated ions into the field-free tube. Upon arrival at the far end of the tube, the ions were discriminated by the respective times of flight and detected by a Channeltron electron multiplier (Galileo Electro Optics). Signals from the detector were recorded and averaged over 1000 sweeps by an oscilloscope (LeCroy 9450), then downloaded and processed. The setup was configured to extract, accelerate and detect positive ions.

2.2.1. Calibration. Primary calibration of the instrument was established from the mass-spectrum obtained by the ablation of 99.9995% pure graphite rod (Alfa Aesar). Fine adjustment of the calibration was achieved using the time-of-flight data from elemental peaks of chromium and cobalt.

2.3. Isotopomer Mass Distribution Simulation. In order to assess isotopomer mass distributions, relative abundances of the isotopomers were calculated using an approach based on polynomial expression expansion[22]. The actual algorithm was implemented through a Visual Basic macro in Microsoft Excel.

2.4. Density Functional Calculations. The DFT calculations were carried out using the Amsterdam Density Functional[23–25] software suite (ADF2012d) with the Perdew-Burke-Ernzerhof (PBE0) functional and the parameterized triplet zeta with double polarization basis set

(TZ2P). The calculations resulted in fully optimized structures in the absence of any symmetry constraints. All possible spin multiplicities were explored and the structures presented in the next subsection are those for the lowest energy cluster. The default program values were employed in the optimization: energy change less than 10^{-4} *Ha* and a gradient less than 10^{-3} *Ha/Å*. Frequency calculations confirmed that the reported structures represent stationary states. Mulliken charges and spin densities were also extracted from the calculations. The bond energies reported here represent the difference between the energy of the cluster and that of the individual atoms (in their electronic ground states).

3. CALCULATIONS

The most likely metallic clusters were Cr_2, Co_2, CoCr, Cr_2Co and $CoCr_2$, and we have modeled these molecules using density functional theory (DFT) calculations. Our geometry and electronic structure results for these molecules are presented in Table 1 and Table 2, respectively. The structures for $CrCo_2$ and $CoCr_2$ are shown in Figure 1. We have modeled the neutral clusters to demonstrate that the formation of the intermetallics is chemically realistic.

Table 1. Geometric parameters for the lowest energy intermetallic clusters.

Cluster	**R_{M1-M2},Å**	**R_{M-M}, Å**	**<M_1-M_2-M_1, deg**	**<M_2-M_2-M_1, deg**
Cr_2	-	1.79	-	-
Co_2	-	1.97	-	-
CrCo	2.25	-	-	-
Cr_2Co	2.46	1.63	38.5	70.7
Co_2Cr	2.46	2.09	50.5	64.8

3.1 Homonuclear clusters.

The two homonuclear dimers have a controversial history involving the possibility of multiple bonding interactions, due to nearly degenerate ground states. The multiconfigurational nature[31] of the homonuclear molecules requires a method such as

Complete Active Space for the ultimate results. However, comparison of our Cr_2 bond lengths with the experimental data in Lombardi and Davis[31], 1.79 vs. 1.68*Å* indicates reasonable agreement and provides confidence in the relative results of the DFT calculation for the additional, previously unreported molecules discussed below. The Cr_2 bond energy of 1.34 is in agreement with the experimental value of 1.53*eV*[31]. There is much less data, experimental or computational, for the cobalt dimer. The calculated and experimental Co_2 bond length data, 1.97 vs. 2.31*Å* are in reasonable agreement. Our calculated bond energy of 5.31*eV* , as is usually observed for DFT calculations, is overestimated, compared to the experimental value of 1.32*eV*[32,33].

Table 2. Bond energies, in eV, symmetries, vertical ionization energies, in eV, and spin multiplicities for the lowest energy intermetallic clusters.

Cluster	**Symmetry**	**Spin Multiplicity**	**Bond Energy (*eV*)**	**Ion. Energy**
Cr_2	$D\infty_h$	1	-1.34	7.97
Co_2	$D\infty_h$	5	-5.16	8.13
CrCo	$C\infty_v$	4	-2.69	14.8
Cr_2Co	C_{2v}	4	-4.38	5.87
Co_2Cr	C_{2v}	2	-6.24	10.8

The chromium dimer experiences antiferromagnetic coupling resulting in a singlet ground electronic state, while the coupling in the cobalt dimer is weak; the ground state has a quintet multiplicity.

3.2 Heteronuclear clusters. The heteronuclear clusters also show large binding energies, and while these may be overestimated, they are all negative at room temperature, supporting the expectation that these clusters will be observed in the TOF spectrometer. The three-atom clusters adopt a triangular conformation under all conditions tested, with the Cr-Cr bond being

shorter than the Co-Cr bond, consistent with the homonuclear clusters. Symmetry unconstrained optimizations of linear structures reverted to the C_{2v} structures shown in the figure.

It appears that the homonuclear antiferromagnetic coupling characteristics carry over to the

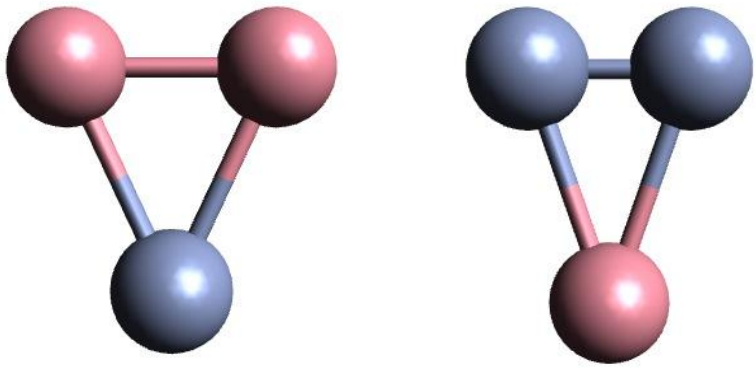

Figure 1. Lowest energy conformers of $CrCo_2$ (left) and $CoCr_2$ (right).

mixed cluster. The CrCo molecule has a quartet ground state, indicating three unpaired electrons from a total of nine from the two isolated metal atoms. The calculations indicate that most of the spin density is in orbitals that are localized on the chromium atom. In the Cr_2Co trimer, the spin density is localized on the cobalt atom, perhaps indicative that the antiferromagnetic coupling in the Cr_2 molecule persists after the addition of the cobalt atom. In contrast, the spin density in the Co_2Cr molecule is spread across the cobalt atoms and the chromium approximately equally.

4. EXPERIMENTAL RESULTS AND DISCUSSION

4.1. Survey spectrum. The mass-spectrum obtained by laser ablation of the Co-Cr alloy sample is presented in Figure 2.. The spectrum exhibits peaks from four groups of cations: (1)

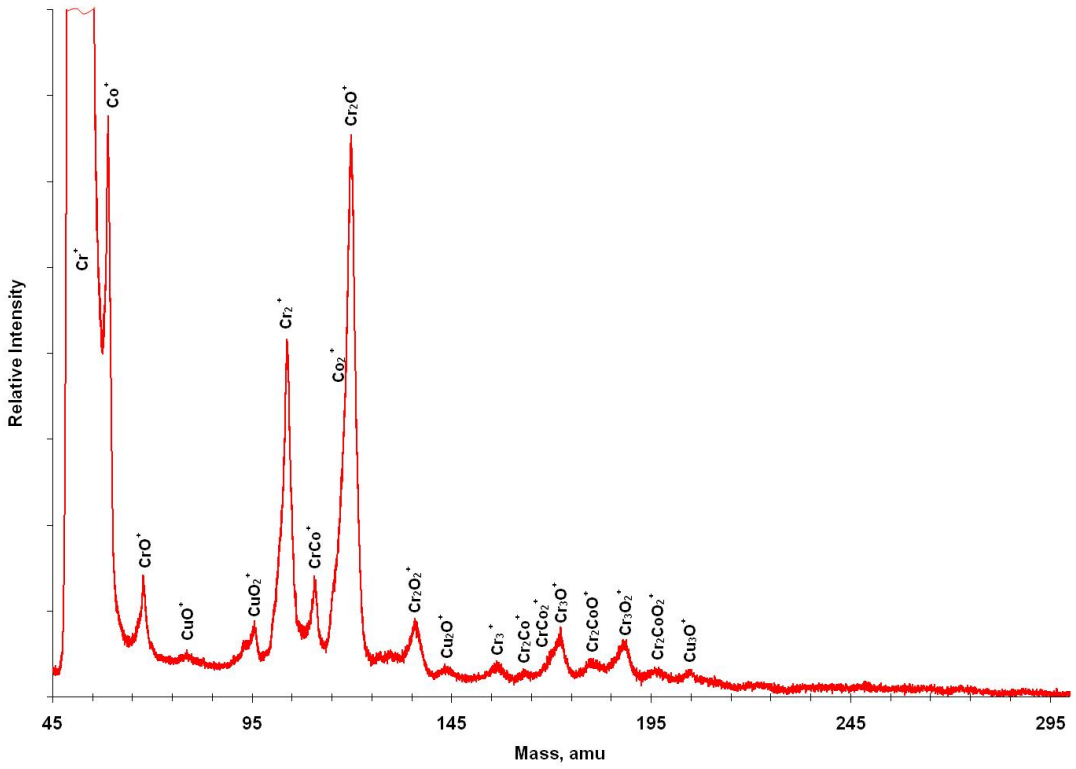

Figure 2. Mass-spectrum obtained from laser ablation of 50/50 at.% chromium and cobalt alloy.

homonuclear metal clusters, (2) binary metal clusters, (3) metal oxide clusters and (4) binary metal oxide clusters. A detectable amount of copper from the die had dissolved into the alloy during synthesis. In addition to the copper contamination, there are several metal oxide peaks that are likely due to the oxygen dissolved in metals. This will be discussed in later sections.

In addition to peak broadening intrinsic to the instrument, there is broadening due to the isotopomeric effect. The abundances of the isotopes that contribute to a particular cluster mass range are summarized in Table 3. These values were also used to simulate isotopomer mass distributions.

Table 3. Natural abundances of the elements (values rounded to the second decimal digit) [26].

Element	**Mass, *amu***	**Abundance, % *at.***
Oxygen	16	99.76
	17	0.04
	18	0.20
Chromium	50	4.35
	52	83.79
	53	9.50
	54	2.37
Cobalt	59	100
Copper	63	69.17
	65	30.83

4.2. Homonuclear Metal Clusters. Peaks in the 50-54 *amu* range originate from chromium isotope ions and the peak at 59 *amu* belongs to the single isotope of cobalt ion. An interesting feature of the mass-spectrum is that the chromium peak is about 18 times the area of the cobalt peak. Several mass-spectra were obtained by ablation of samples cut from different locations of the ingot to determine if this was due to inhomogeneity of the target, but all samples demonstrated consistent results. This phenomenon can be attributed to the large difference in the ionization potentials of chromium and cobalt, 6.77 and 7.88 *eV*, respectively [27]. The latter can also explain the absence of cobalt-oxygen clusters in the spectrum: cobalt is more electronegative element than chromium, thus, the latter is more likely to share the electrons with oxygen, given that the detected cationic clusters are inherently electron deficient.

Peaks with maxima at 104 and 156 *amu* are attributed to the chromium dimer, Cr_2^+, and trimer, Cr_3^+, respectively. The cobalt dimer, Co_2^+, peak was not clearly resolved due to overlap with the Cr_2O^+ peak.

4.2. Binary Metal Clusters. The peak at 111 *amu* reveals formation of the $CrCo^+$ binary ion. To the best of our knowledge this is the first evidence of the formation of such a molecule. Although there is an isotopomer of the CuO_3^+ cluster with the same mass, a contribution from this ion was ruled out by several methods. First, the presence of CuO_3^+ would also result in a noticeable satellite peak at 113 *amu* due to another isotopomer of this cluster as shown in Figure 3, which presents simulated mass-multiplets for both $CrCo^+$ and CuO_3^+. This simulation also

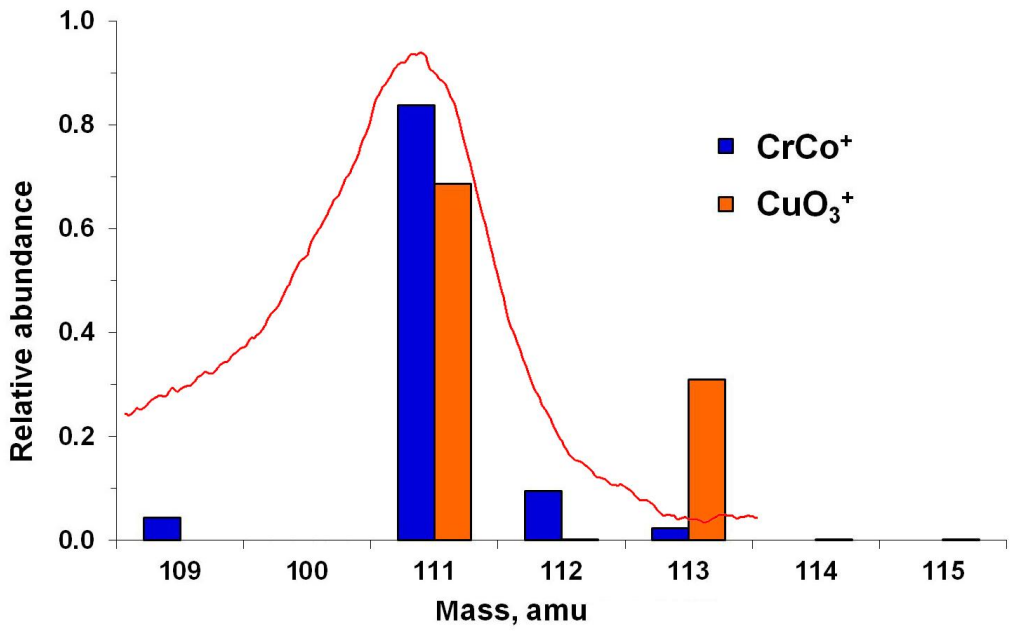

Figure 3. Comparison of the isotopomer mass distribution for $CrCo^+$ and CuO_3^+. The red line shows a running average of mass-spectrum signal intensity

shows the shapes of the multiplets to be inconsistent with the presence of CuO_3^+. The CuO_3^+ multiplet is weighted towards heavier mass from the peak at111 *amu* while the $CrCo^+$ multiplet ranges between 109-113 *amu* and is almost symmetric around 111 *amu*. Lastly, an earlier TOF-MS study on the synthesis of copper-oxygen clusters by laser ablation of copper oxides showed no indication of CuO_3^+ formation.[28]

We also detect a Cr_2Co^+ binary metal cluster formation indicated by a peak at 163 *amu* with a span over the 159-167 *amu* range. Figure 4 illustrates simulated isotopomer mass distributions for this cluster.

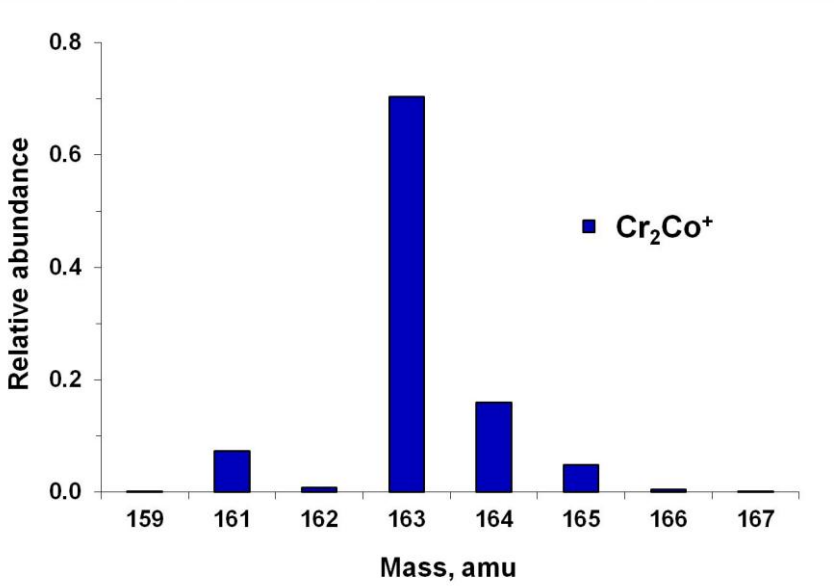

Figure 4. Isotopomer mass distributions for the Cr_2Co^+ cluster.

Lastly for this family of ions, there is possible evidence of $CrCo_2^+$ cluster formation in the 168-172 *amu* range with a maximum at 170 *amu*. Unfortunately, it overlaps with the Cr_3O^+ 172 *amu* peak ranging between 166 and 180 *amu* and this appears as a low-mass shoulder on this peak. Isotopomer mass distributions for both ions are compared in Figure 5. In order to approximate the bimodal fit of both distributions into the mass-spectrum the abundances of $CrCo_2^+$ isotopomers were scaled by a factor of 0.4.

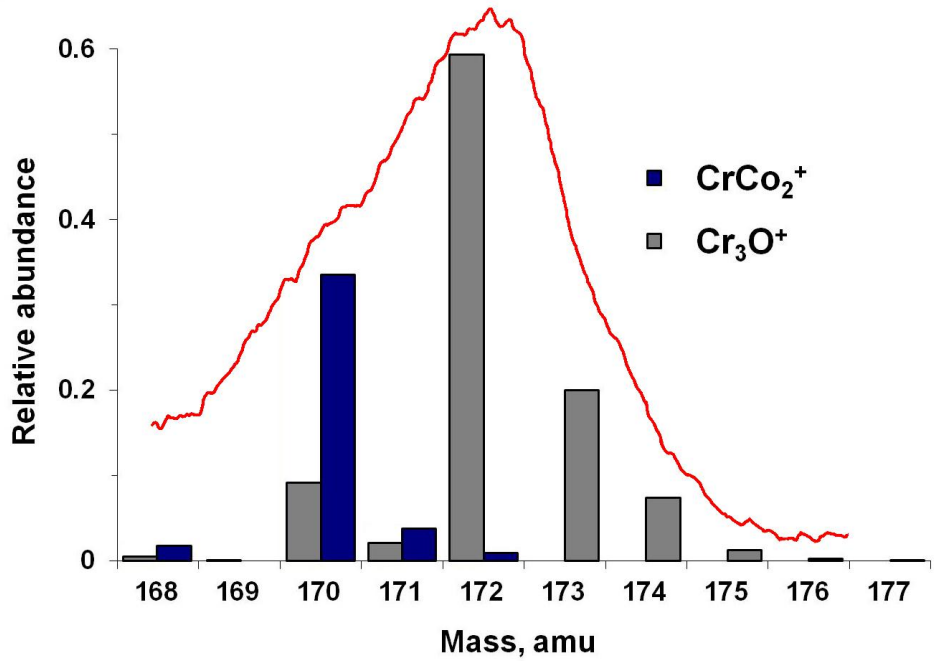

Figure 5. Isotopomer mass distribution of $CrCo_2^+$ and Cr_3O^+ clusters ($CrCo_2^+$ isotopomer abundances are scaled by factor of 0.4). The red line shows a running average of mass-spectrum signal intensity.

4.3. Metal Oxide Clusters. Despite precautions to maintain a low- oxygen environment during both arc-melting (argon purge) and mass spectrometry (10^{-6} *Torr* vacuum), many oxide clusters were detected. As was mentioned above, the presence of oxygen was attributed to its reactivity with metals, including the chromium and cobalt materials used to synthesize the alloy as well as the copper die.

Among oxygen containing clusters the detected monocopper ions included CuO^+, 79-81 *amu*, and CuO_2^+, 95-97 *amu*. Only one dicopper cluster Cu_2O^+, 142-148 *amu*, was registered. At the upper end of the spectrum there is a peak around 207 *amu* indicating the presence of tricopper cluster, Cu_3O^+, which has extraordinary stability according to Ma, *et al.*[28].

Several chromium-oxygen clusters were detected starting with the lightest member of this family CrO^+ at 68 *amu*. This ion was previously described in work by Aubriet *et al.*[29] The next observed set, dichromium oxide clusters Cr_2O^+ at 120 *amu* and $Cr_2O_2^+$ at 136 *amu* were also

mentioned in ref. 22. The authors performed laser ablation of various chromium oxides and also obtained dichromium clusters richer in oxygen, for example $Cr_2O_3^+$, $Cr_2O_4^+$ *etc*. These clusters did not form in our experiments. In contrast to Aubriet's work we detected metal-rich, trichromium oxide clusters: Cr_3O^+ at 172 *amu* and $Cr_3O_2^+$ at 188 *amu*.

Cobalt, the most electronegative of the three metals at play in cluster formation in our experiments, did not form detectable amounts of any oxide clusters reported in work by Dibble *et al.* [30]

4.4. Binary Metal Oxide Clusters. While there were no cobalt oxide clusters observed in the ablation plume, two types of clusters containing chromium, cobalt and oxygen did form: dichromium cobalt oxide clusters Cr_2CoO^+ and $Cr_2CoO_2^+$ according to the peaks at 197 *amu* and 181 *amu*, respectively.

5. CONCLUSIONS

In this study, we observed the formation of a large variety of clusters, including the desired $CoCr^+$ species. Clusters with copper and oxygen are attributed to impurities in the target. Singly ionized Cr^+ ions dominated the sp**e**ctrum, with Cr_2^+ and Cr_2O^+ also in abundance. A well-resolved peak for $CoCr^+$ was observed, along with smaller peaks for $CoCr_2$ and Co_2Cr. DFT calculations indicate that all of the observed intermetallic clusters are thermodynamically favorable, therefore, their presence in the mass spectrometer is an rational result. Given the high temperatures in the laser ablation process, the relative magnitudes of the exoergicity are not expected to be manifested in the ratio of peak heights.

While the flux of the $CoCr^+$ cluster was small in our setup, this, or other generation methods such as sputtering, followed by a quadrupole mass analyzer should make it possible to deliver binary clusters to the film growth surface in a vacuum deposition system. This will permit the

direct incorporate these clusters into a dielectric or semiconducting film co-deposited from a separate source. The low adatom mobility of the transition metals, and the observed stability of the clusters should assure that the dopants retain their proximity in the resulting dual-doped film. Comparison of the optical properties of these films with randomly co-deposited dopants will permit detailed examination of proximity effects in charge-transfer processes.

AUTHOR INFORMATION

Corresponding author

Ursula J. Gibson *ursula.gibson@ntnu.no*

Author Contributions

The manuscript was written through contributions of all authors. All authors have given approval to the final version of the manuscript.

ACKNOWLEDGEMENTS: The authors gratefully acknowledge support from the Research Council of Norway, NOTUR, and Dartmouth College.

REFERENCES

(1) Schliesser, A.; Picqué, N.; Hänsch, T. W. Mid-Infrared Frequency Combs. *Nat. Photonics* **2012**, *6*, 440–449.

(2) Chaney, C. A.; Yang, Y.; Fried, N. M. Hybrid Germanium/silica Optical Fibers for Endoscopic Delivery of erbium:YAG Laser Radiation. *Lasers Surg. Med.* **2004**, *34*, 5–11.

(3) Sorokina, I. T.; Sorokin, E.; Mirov, S.; Fedorov, V.; Badikov, V.; Panyutin, V.; Schaffers, K. I. Broadly Tunable Compact Continuous-Wave Cr(2+):ZnS Laser. *Opt. Lett.* **2002**, *27*, 1040–1042.

(4) Jackson, S. D. Cross Relaxation and Energy Transfer Upconversion Processes Relevant to the Functioning of 2 Mm Tm3+-Doped Silica Fibre Lasers. *Opt. Commun.* **2004**, *230*, 197–203.

(5) Bartolacci, C.; Laroche, M.; Robin, T.; Cadier, B.; Girard, S.; Gilles, H. Effects of Ions Clustering in Nd3+/Al3+-Codoped Double-Clad Fiber Laser Operating near 930 Nm. *Appl. Phys. B* **2010**, *98*, 317–322.

(6) Arai, K.; Namikawa, H.; Kumata, K.; Honda, T.; Ishii, Y.; Handa, T. Aluminum or Phosphorus Co-doping Effects on the Fluorescence and Structural Properties of Neodymium-doped Silica Glass. *J. Appl. Phys.* **1986**, *59*, 3430–3436.
(7) Jackson, S. D. Towards High-Power Mid-Infrared Emission from a Fibre Laser. *Nat. Photonics* **2012**, *6*, 423–431.
(8) Yan, W.; Sun, Z.; Liu, Q.; Yao, T.; Jiang, Q.; Hu, F.; Li, Y.; He, J.; Peng, Y.; Wei, S. Mediating Distribution of Magnetic Co Ions by Cr-Codoping in (Co,Cr): ZnO Thin Films. *Appl. Phys. Lett.* **2010**, *97*, 042504.
(9) Knight, W.; Clemenger, K.; Deheer, W.; Saunders, W.; Chou, M.; Cohen, M. Electronic Shell Structure and Abundances of Sodium Clusters. *Phys. Rev. Lett.* **1984**, *52*, 2141–2143.
(10) Fowler, P. W. How Unusual Is C60? Magic Numbers for Carbon Clusters. *Chem. Phys. Lett.* **1986**, *131*, 444–450.
(11) Burnin, A.; Sanville, E.; BelBruno, J. J. Experimental and Computational Study of the ZnnSn and ZnnSn+ Clusters. *J. Phys. Chem. A* **2005**, *109*, 5026–5034.
(12) Zhou, Z.-J.; Hu, Y.-F. Structures, Stabilities, and Electronic Properties of Gold Silicide Clusters: Comparison with Pure Silicon Clusters. *Z. Naturforschung Sect. - J. Phys. Sci.* **2012**, *67*, 99–110.
(13) Teghil, R.; D'Alessio, L.; Santagata, A.; Zaccagnino, M.; Ferro, D. Pulsed Laser Ablation of MoSi2: Gas Phase Analysis. *Appl. Surf. Sci.* **2002**, *186*, 335–338.
(14) Yamada, Y.; Deng, H.; Snyder, E.; Castleman, A. Copper Antimony and Copper Bismuth Alloy Clusters - Magic Numbers and Electronic-Structure. *Chem. Phys. Lett.* **1993**, *203*, 330–336.
(15) Liu, Z.; Wang, C.; Huang, R.; Zheng, L. Mass Distributions of Binary Aluminum Cluster Anions Al(n)x(m)(-) (x=o, S, P, As, C). *Int. J. Mass Spectrom. Ion Process.* **1995**, *141*, 201–208.
(16) Waller, S. E.; Mann, J. E.; Jarrold, C. C. Asymmetric Partitioning of Metals among Cluster Anions and Cations Generated via Laser Ablation of Mixed Aluminum/Group 6 Transition Metal Targets. *J. Phys. Chem. A* **2013**, *117*, 1765–1772.
(17) Martin, T. P. Compound Clusters. II. Intermetallics and Phosphides. *J. Chem. Phys.* **1985**, *83*, 78–84.
(18) Biswas, K.; Das, P. K.; Chattopadhyay, K. Microstructural Evolution and Metastable Phase Formation in Laser Ablation-Deposited Films of Fe-Rich Fe-Ge Intermetallic Compounds. *Philos. Mag.* **2007**, *87*, 307–323.
(19) McIndoe, J. S. Laser Synthesis of Transition Metal Clusters. *Transit. Met. Chem.* **2003**, *28*, 122–131.
(20) Bluiett, A. G.; Condon, N. J.; O'Connor, S.; Bowman, S. R.; Logie, M.; Ganem, J. Thulium-Sensitized Neodymium in KPb2Cl5 for Mid-Infrared Laser Development. *J. Opt. Soc. Am. B-Opt. Phys.* **2005**, *22*, 2250–2256.
(21) Braud, A.; Girard, S.; Doualan, J. L.; Moncorge, R. Spectroscopy and Fluorescence Dynamics of (Tm/sup 3+/,Tb/sup 3+/) and (Tm/sup 3+/,Eu/sup 3+/) Doped LiYF/sub 4/ Single Crystals for 1.5-Mm Laser Operation. *IEEE J. Quantum Electron.* **1998**, *34*, 2246–2255.
(22) Burnin, A.; BelBruno, J. J. SCnS Linear Chain Production by Direct Laser Ablation. *J. Phys. Chem. A* **2003**, *107*, 9547–9553.
(23) Velde, G.; Baerends, E. Precise Density-Functional Method for Periodic Structures. *Phys. Rev. B* **1991**, *44*, 7888–7903.
(24) Wiesenekker, G.; Baerends, E. Quadratic Integration Over the 3-Dimensional Brillouin-Zone. *J. Phys.-Condens. Matter* **1991**, *3*, 6721–6742.
(25) *BAND2013 Theoretical Chemistry, Vrije Universiteit, Amsterdam, The Netherlands,*.
(26) Haynes, W. M, Editor. *CRC Handbook of Chemistry and Physics, 94th Edition (Hardback) - Taylor & Francis*; 94th ed.; Taylor and Francis.
(27) Sansonnetti J.E.; Martin W. C. *Handbook of Basic Atomic Spectroscopic Data*; National Institute of Standards and Technology.

(28) Ma, C. S.; Li, H. Y.; Zhang, X. G.; Bai, J. L.; Wang, X. Y.; Wang, L.; Zhang, G. Q.; He, G. Z.; Lou, N. Q. Formation of Copper Oxide Cluster Ions - Copper Oxide Cluster Ions Generated by Direct Laser Ablation of Copper Oxide Solid. *Prog. Nat. Sci.* **1996**, *6*, 159–164.
(29) Aubriet, F.; Maunit, B.; Courrier, B.; Muller, J. F. Studies of the Chromium Oxygenated Cluster Ions Produced during the Laser Ablation of Chromium Oxides by Laser Ablation Ionization Fourier Transform Ion Cyclotron Resonance Mass Spectrometry. *Rapid Commun. Mass Spectrom.* **1997**, *11*, 1596–1601.
(30) Dibble, C. J.; Akin, S. T.; Ard, S.; Fowler, C. P.; Duncan, M. A. Photodissociation of Cobalt and Nickel Oxide Cluster Cations. *J. Phys. Chem. A* **2012**, *116*, 5398–5404.
(31) Lombardi, J. R.; Davis, B. Periodic Properties of Force Constants of Small Transition-Metal and Lanthanide Clusters. *Chem. Rev.* **2002**, *102*, 2431–2460.